Electrochimica Acta 346 (2020) 136285

Contents lists available at ScienceDirect

Electrochimica Acta

journal homepage: www.elsevier.com/locate/electacta

Study of oxygen electrode reactions on symmetrical porous $SrTi_{0.30}Fe_{0.70}O_{3-\delta}$ electrodes on $Ce_{0.8}Gd_{0.2}O_{1.9}$ electrolyte at 800 °C–500 °C

Aleksander Mroziński *, Sebastian Molin , Piotr Jasiński

Laboratory of Functional Materials, Faculty of Electronics, Telecommunications and Informatics, Gdańsk University of Technology, ul. G. Narutowicza 11/12, 80-233, Gdańsk, Poland

ARTICLE INFO

Article history:
Received 15 February 2020
Received in revised form
17 April 2020
Accepted 20 April 2020
Available online 21 April 2020

Keywords:
Solid oxide cells
Oxygen electrodes
Mixed ionic electronic conductor
Impedance spectroscopy
Distribution of relaxation times

ABSTRACT

Iron doped strontium titanates ($SrTi_{1-x}Fe_xO_{3-\delta}$) are an interesting mixed ionic-electronic conductor model used to study basic oxygen reduction/oxidation reactions. In this work, we performed an impedance spectroscopy study on symmetrical porous $SrTi_{0.30}Fe_{0.70}O_{3-\delta}$ (STF70) electrodes on a ceria-based electrolyte. The sample was measured in varying oxygen concentration: from 0.3% to 100% in 800 °C–500 °C temperature range. Low polarisation resistance (e.g. <125 mΩ cm^2 at 600 °C in the air) values were obtained, showing an overall high performance of the STF70 electrode. Impedance data analysis was assisted by the distribution of relaxation times method, which allowed an equivalent electrical circuit to be proposed comprising of two resistance/constant phase element sub-circuits connected in series. The medium frequency contribution, with a characteristic frequency of ~2000 Hz at 800 °C in air, originates most probably from possible surface diffusion followed by charge transfer reaction limitation, whereas the lower frequency contribution (characteristic frequency <10 Hz) is due to gas-phase diffusion.

1. Introduction

Electrochemical impedance spectroscopy (EIS) is a powerful method for the determination of the electrochemical properties of materials in an almost unlimited number of applications. For example, EIS is used extensively to determine the performance of electrodes in solid oxide cells (SOCs) [1–3], in biosensors [4–6], in oxygen sensors [7], in pH sensors [8,9] or determining properties of conductive polymers like polypyrrole [10,11]. In the case of SOCs, the polarisation resistance of the electrodes is usually measured as a function of the materials preparation methodology (e.g. sintering temperature, particle size, resulting porosity), measurement temperature, and oxygen partial pressure. Often, the frequency response (impedance spectra) of the electrodes shows quite a complex result, not easily fitted with simple circuits. Over the years, useful tools have been developed to help in the analysis of these complex phenomena. The method that has been growing in popularity in recent years is the distribution of relaxation times (DRT) analysis [12–18]. It became popular due to the availability of a free software tool developed by the prof. Ciucci group – DRTTools [19–23]. The software offers simple control over the most important parameters required to successfully and reliably use the DRT method.

DRT offers the possibility of differentiation of the measured spectra of several electrochemical processes when characteristic frequencies overlap. Quite a few research groups have used this tool to analyse the electrodes of SOCs. Both the oxygen and fuel electrodes were studied to devise their mechanisms.

Płończak et al. used DRT to determine the electrochemical processes on thin-film dense (La,Sr)$MnO_{3-\delta}$ electrodes. DRT allowed the number of contributing processes to be resolved. For a description of the symmetrical electrode system, three R-CPE elements connected in series were used (with characteristic frequencies at 900 °C of ~1 kHz, ~30 Hz, and 1500 Hz). Clematis et al. analysed $Ba_{0.5}Sr_{0.5}Co_{0.8}Fe_{0.2}O_{3-\delta}$ oxygen electrodes. DRT was used to determine the effects of electrode polarisation in a 3-electrode cell, allowing the polarisation influenced processes to be seen. In addition to the oxygen electrode, fuel electrodes were also studied [15,24–26]. DRT can also be used to study full fuel cells, where

* Corresponding author.
E-mail address: aleksander.mrozinski@pg.edu.pl (A. Mroziński).

https://doi.org/10.1016/j.electacta.2020.136285

there are many simultaneous electrochemical reactions. Chrzan et al. studied a solid oxide cell with infiltrated electrodes and the effects of ageing. As many as 5 different processes were determined [27]. Tong et al. studied large-area cells with $La_{0.6}Sr_{0.4}CoO_{3-\delta}$ electrodes. A full cell model with 5 contributing processes was also devised based on DRT analysis [28]. Also, full polymer electrolyte cells were studied using DRT. The analysis revealed as many as 7 contributions. Moreover, DRT can be used in batteries and other systems [29,30].

Oxygen electrode reactions, including oxygen reduction and oxidation reactions, are one of the most important chemical/electrochemical reactions studied. Even though these processes have been studied for many years, there is still no specific and universal model for the reactions at high temperatures. Due to the complex nature of the process, it is highly dependent on the conditions (temperature, oxygen concentration), as well as on the material and its preparation (defects, particle size, etc). Developing reliable tools for the determination of the electrochemical processes is an important and challenging task.

A reversible oxygen electrode reaction is a complex process consisting of several elementary steps. One possible pathway for the reaction is presented below (according to Kröger-Vink notation) [31,32]:

Step 1) Mass transfer of O_2 molecules in the gas phase and adsorption on the electrode surface: $O_{2(g)} \leftrightarrow O_{2(ads)}$;
Step 2) Dissociation of the adsorbed molecules: $O_{2(ads)} \leftrightarrow 2O_{(ads)}$;
Step 3) Charge transfer to oxide ion electrolyte: $O_{(ads)} + 2e^- + V_{\ddot{O}} \leftrightarrow O_O^x$;
Step 4) Mass transfer of oxide ions in the bulk of the electrode/electrolyte: $V_{\ddot{O}(electrode)} \leftrightarrow V_{\ddot{O}(electrolyte)}$;

To determine the rate-limiting step of the oxygen electrode reaction, the electrode resistance can be studied as a function of both temperature and oxygen partial pressure (pO_2) [33]. The following generalised relation can be used to describe the electrode resistance (R_{el}):

$$\frac{1}{R_{el}} \propto (pO_2)^n \qquad \text{[Equation 1]}$$

Different n-values indicate the type of oxygen species involved in the electrochemical reaction [33–35]. An inverse proportionality relation (n = 1) indicates the molecular oxygen involved (O_2), a $(pO_2)^{0.5}$ dependence indicates the contribution of atomic oxygen (O). The value of n = 3/8 is possibly related to the partial reduction of the atomic oxygen ($O_{(ads)} + e^- \rightarrow O^-_{ads}$). For n = 1/4, the charge transfer reaction has been described as the limiting factor. The studies of electrode polarisation as a function of both the temperature and oxygen concentration are thus a powerful tool to determine the rate-determining reactions. These are however generally complex measurements which can be affected by many factors [36,37], thus the results should be treated with caution.

Iron substituted strontium titanates, with a general formula of $SrTi_{1-x}Fe_xO_{3-\delta}$ are model materials used for studies of mixed ionic-electronic conductors [36,38–40]. Depending on the iron content, the properties of the materials (electrical conductivity, surface exchange, and diffusion coefficient) can be altered and their effects studied [41,42]. These materials have been shown to offer promising performance as catalysts for a number of reactions [43,44], as oxygen electrodes for solid oxide cells [45,46], and found use in resistive oxygen gas sensors [47,48]. Our previous study of the electrochemical processes on porous $SrTi_{0.65}Fe_{0.35}O_{3-\delta}$ (STF35) electrodes revealed three different contributions. For a description of the high-frequency contribution (characteristic frequency of ~200 Hz at 800 °C in air), a diffusion related Gerischer equivalent element was used. It was ascribed to the diffusion of the oxygen ion in the STF35. Based on this work, it is interesting to study the individual contributions for higher Fe-substituted materials, which have higher total electrical conductivities, lower band gaps and higher oxygen vacancy concentrations [36,42,49].

In this work, we study $SrTi_{0.30}Fe_{0.70}O_{3-\delta}$ perovskite for its oxygen electrode reaction processes based on porous symmetrical electrode configurations. STF70 is an interesting electrode material with high ionic conductivity, catalytic activity, and moderate electronic conductivity. By application of electrochemical impedance spectroscopy coupled with the distribution of relaxation times analysis, we determine the equivalent circuit and then obtain the individual contributions and follow their temperature and oxygen concentration dependent behaviour. This allows for the determination of the rate-limiting processes and opens the possibilities to improve the materials in the future.

2. Experimental

$SrTi_{0.30}Fe_{0.70}O_{3-\delta}$ (STF70) powders were fabricated by a solid state reaction method, according to the details in Ref. [46,50]. Stoichiometric amounts of reagent grade $SrCO_3$, TiO_2 (EuroChem, Poland), and Fe_2O_3 powders (Chempur, Poland) were weighed and mixed in a planetary ball mill (Fritsch Pulverisette7). The mixed powders were pressed into a large pellet (diameter of ~3 cm, thickness ~1.5 cm), calcined at 1200 °C for 15 h, followed by crushing, pressing of a new pellet and calcining again at 1200 °C to form the single phase material. To measure the electrical conductivity of the bulk STF70, a pellet was prepared by compacting a powder and sintering at 1200 °C for 2 h. To obtain fine-grained powder for paste preparation, it was milled in a planetary mill with ZrO_2 balls for 12 h and thermally treated at 600 °C. From the powder, the electrode paste was prepared. The powder was mixed with a commercial paste vehicle (403, ESL, USA) in a weight ratio of 2:3. The paste was mixed in a planetary ball mill with zirconia balls.

For symmetrical electrode substrates, $Ce_{0.8}Gd_{0.2}O_{1.9}$ (CGO) pellets were prepared. Commercial CGO powder (DKKG, Japan) was pressed into cylindrical pellets of ~1 mm thickness and 16 mm diameter. No additives were used for pressing. The green pellets were sintered at 1400 °C for 8 h. The porosity of the pellets after the sintering was <4% measured by Archimedes method. After the sintering, the planar surfaces of the CGO pellets were polished using diamond suspensions (particle size ~3 μm). After the polishing step, the individual pellets had a thickness of ~600 μm.

Electrical conductivity measurements of the bulk CGO and STF70 pellets were performed using the van der Pauw method. Platinum wires were fixed to the sample outer edges by silver paste (DuPont 4922 N, USA). The measurement was performed using Keithley 2400 and an automated data logging system in the temperature range of 900–450 °C in 100% O_2, 20% O_2, and 1% O_2 for the STF70 and CGO.

Using the pre-prepared paste and the CGO pellets, symmetrical electrode samples were produced. The electrodes were screen-printed (DEK 65, UK) on the two sides and sintered at 800 °C for 2 h. The resulting electrode area was 0.4 cm^2. For current collection, the surfaces of the electrodes were painted with Pt paste (ESL 5542, USA), dried and fired at 600 °C. The surface roughness of the electrodes was measured using a Keyence laser scanning microscope.

The impedance measurements were performed in a 4-wire compression cell with Au meshes pressed against the STF70/Pt electrodes. The measurement cell was placed inside a sealed quartz tube in order to control the atmosphere. A Novocontrol Alpha-A

with a ZG-4 interface was used for measurement of the impedance spectra. Analyses were carried out at 25 mV amplitude in the frequency range of 3 MHz to 0.05 Hz. The temperatures were 800 °C, 700 °C, 600 °C, and 500 °C. A controlled oxygen concentration (100%, 80%, 50%, 30%, 20%, 15%, 10%, 5%, 2.5%, 1%, 0.3%) was obtained by mixing high precision reference gas mixtures (oxygen in argon): 100%, 20%, 1%, and 0.01% (100 ppm) using mass flow meters (Aalborg, USA).

For plotting and analysis of the impedance data, the obtained impedance spectra were re-calculated for the electrode area (0.4 cm^2). In the case of polarisation resistance, the value was further divided by a factor of 2 to accommodate the two identical, symmetrical interfaces.

Impedance spectra were fitted using the Elchemea Analytical web-tool developed by the Technical University of Denmark (www.elchemea.com, DTU Energy).

The collected impedance spectra were analysed by the distribution of relaxation times method. For this purpose, the freely available DRTTool from the prof. Ciucci group was utilised. Prior to use, the spectra were corrected for the inductance of the rig. Different parameters for the DRT were used to evaluate the spectra, as described in the results section.

The microstructural characterisation of the electrodes was performed by scanning electron microscopy (SEM) using a Thermo Fischer Phenom XL microscope with an integrated energy dispersive x-ray spectrometer. For analysis of the cross-sections, the samples were vacuum embedded (CitoVac, Struers) in epoxy (EpoFix, Struers) and polished down to a 1 μm finish.

3. Results and discussion

3.1. Sample general properties

The microstructure of the symmetrical STF70 electrodes on the CGO electrolyte is shown in Fig. 1A and B. Screen-printing of the electrodes results in a macroscopically uniform microstructure of the electrodes. Higher magnification images reveal the thickness of the electrodes to be ~20 μm, with a porosity of ~35%. The particles visible in the electrodes have sub-micrometre sizes. The surface roughness parameter value, $S_a = 0.41$ μm, confirms a smooth surface. The remnants of the painted Pt current collector are still visible. The thickness of the CGO pellet is ~600 μm, which was also measured with micro-caliper. The sample shown had already undergone the measurement procedure, which included several thermal cycles and many oxygen concentration changes. The microstructure shows no sign of cracks or delamination, which indicates good compatibility of the STF70 with the CGO substrate, even though a mismatch of thermal expansion coefficient (TEC) exists. The previously measured TEC of the bulk STF70 is ~23×10^{-6} K^{-1} [50], whereas the TEC of the CGO is ~13×10^{-6} K^{-1}. The difference in TEC values is high (~10×10^{-6} K^{-1}), but some other electrode materials with such a large TEC mismatch are successfully used (e.g. $La_{0.6}Sr_{0.2}Co_{0.2}Fe_{0.8}O_{3-\delta}$, $La_{0.6}Sr_{0.4}CoO_{3-\delta}$ with TECs >18 [51,52]).

The total electrical conductivities of the bulk CGO and STF70 materials were measured on sintered pellets by the van der Pauw method, and the results are presented in Fig. 2A. The electrical conductivity of ceria, representing purely ionic O^{2-} conduction, is much lower than the conductivity of the iron substituted strontium titanate, which is a mixed ionic-electronic conductor. At 800 °C, the ionic conductivity of ceria is ~100 mS cm^{-1}, and decreases to ~5 mS cm^{-1} at 500 °C, with an activation energy of 0.69 eV. These are typical values for doped ceria electrolytes [53]. The measured total conductivity of STF70 in air is ~16 S cm^{-1} in air at 800 °C. For STF70, the exact ionic and electronic conductivity contributions are not specifically reported. Based on the results of a series of iron substituted strontium titanates, the electronic transference number is ~0.98, with the ionic conductivity at the level of ~40 mS cm^{-1} at 800 °C [54]. As presented in Fig. 2A, the electrical conductivity of CGO, in this oxygen partial pressure range (0.3%–100% O_2), due to the ionic regime of operation, is not dependent on the oxygen concentration [53]. STF70 is a typical p-type conductor, with its electronic conductivity increasing with increasing oxygen content (in the high pO_2 range). According to Ref. [42], in the temperature range 750 °C–1000 °C, based on the defect chemistry description, the total electrical conductivity follows the conductivity ~ $(pO_2)^{1/4}$ behaviour, which indicates that the oxygen vacancy concentration is independent of the partial pressure. Thus the mobility/concentration changes of the majority carriers (p-type) dominate the total conduction of STF70 in the studied oxygen concentration range.

Fig. 2B and C summarise the results obtained from the impedance measurements on the symmetrical electrodes. The data is divided into the ohmic - R_s (Fig. 2B) and polarisation - R_{pol} (Fig. 2C) contributions, shown for three oxygen levels (100%, 20%, and 1%). The spectra and underlying electrochemical processes will be analysed in detail in the following sections. From Fig. 2B and C, it is evident that the oxygen concentration change has a negligible influence on the ohmic part, and a large influence on the polarisation contribution.

3.2. Impedance spectra and distribution of relaxation times analysis

For assistance in the determination of the electrochemical processes occurring on the STF70 electrodes, the DRT method was used for impedance spectra analysis. At the first step, we tried to vary the analysis parameters in order to obtain satisfactory results. A representative spectrum, used as a model example here, measured at 800 °C in 1% O_2 is presented in Fig. 3A. The DRT of the presented spectra is shown in Fig. 3B. Different λ parameters (λ – regularisation parameter) were used for qualitative analysis. A

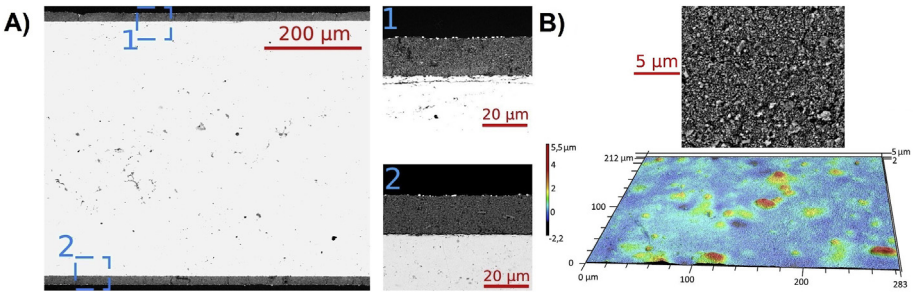

Fig. 1. A) SEM polished cross-section image of the symmetrical STF70 electrodes on CGO electrolyte, B) surface morphology of the STF70 electrode including SEM surface image and laser microscope profilometry.

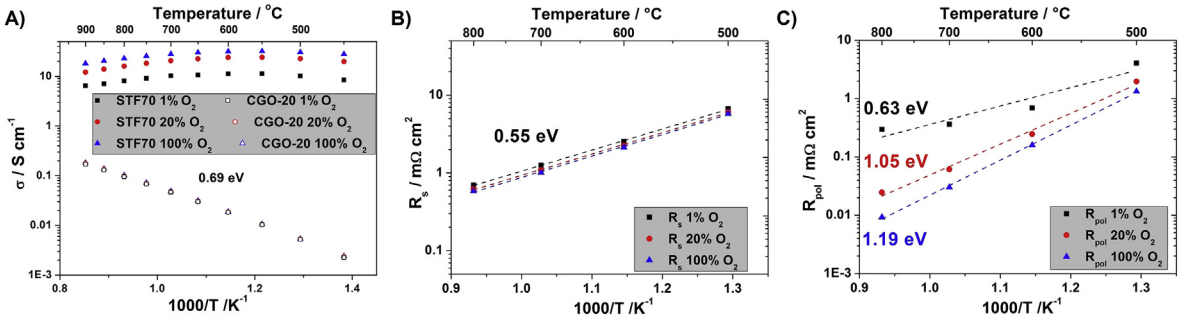

Fig. 2. A) Electrical conductivity of CGO and STF70, B) ohmic, and C) polarisation resistances of the symmetrical STF70 electrodes.

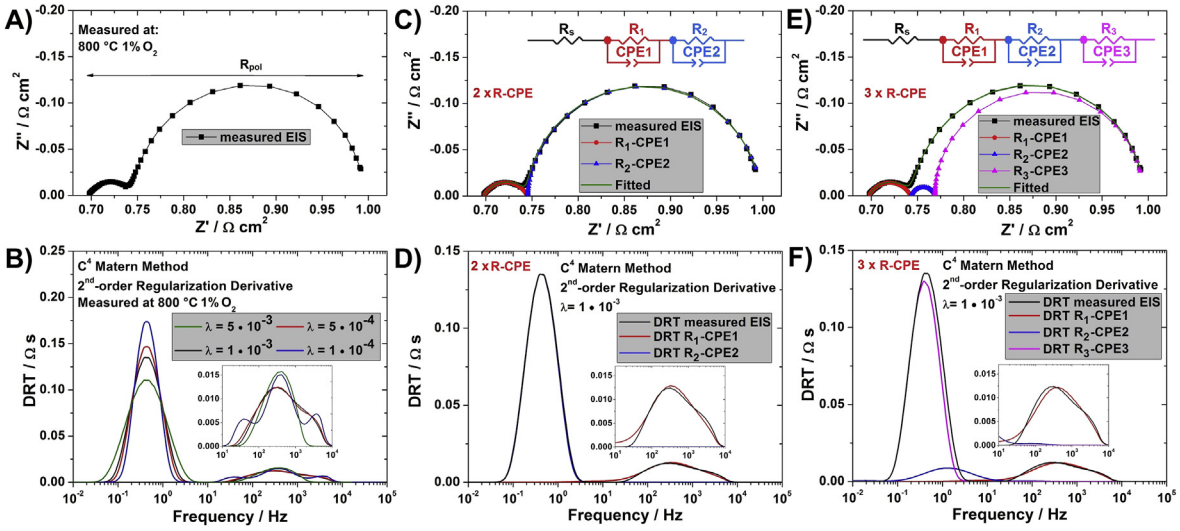

Fig. 3. A) Exemplary impedance spectra measured at 1% O_2 at 800 °C used as a model result, B) the effect of different λ-values on the resulting DRT spectra, C) spectra with fitted two R-CPE elements with D) corresponding DRT analysis, E) spectra with fitted three R-CPE elements with F) corresponding DRT analysis.

change of λ results in the number of "peaks" visible at higher frequencies, and in the lowering and widening of the lower frequency contribution. For $\lambda = 1 \times 10^{-4}$, there are at least three peaks visible around ~300 Hz. Increasing the lambda parameter to 5×10^{-4} and 1×10^{-3} results in a change of shape of the DRT spectra. The process at higher frequencies now seems to have a shoulder at the higher frequencies only. Analysing simulated simple R-CPE elements (not shown here), this broadening of the DRT peaks does not come from another R-CPE contribution, but is just a result of the fitting of a single R-CPE element. For $\lambda = 5 \times 10^{-3}$, only a single broader peak can be found around ~300 Hz. Based on this simple analysis, the selection of λ can have a profound effect on the number of peaks determined by DRT. On the basis of the performed analyses, it was chosen to further study an equivalent circuit consisting of two R-CPE elements connected in series and perform a DRT with $\lambda = 1 \times 10^{-3}$.

Unfortunately, hardly any publications are reporting the specific parameters used for the DRT analysis. For example, Weiß et al. used a value of $\lambda = 1 \times 10^{-5}$, and they obtained and analysed 7 different peaks for a polymer electrolyte cell. For comparison, Heinzmann et al. showed the influence of λ on the resulting DRT spectra for polymer electrolyte membrane cells [55]. They used a value of $\lambda = 1 \times 10^{-3}$, which provided "a compromise between selectivity, low residuals, and oscillation avoidance". For lower λ values, more peaks appeared that were believed to be not true.

Fig. 3C shows the same spectra as Fig. 3A, with added individual contributions calculated according to the developed equivalent circuit consisting of two R-CPE elements. A very good fit is obtained, which is also confirmed by the back-calculation of the DRT based on the fitted R-CPE parameters, as presented in Fig. 3D. To obtain individual R-CPE equivalent circuit values, the complex non-linear least-squares fitting (NLLS) Elchemea software was used. So the DRT was only used to determine the number of equivalent circuit elements. In principle, the DRT can also be used to calculate the contribution resistances (given by the peak area), but this approach is not well proven. As we will briefly show (Fig. 3 and its discussion), DRT transforms the data and can alter it considerably depending on the used parameters, which will influence the fitting procedure results. It would be also problematic for non-trivial elements, for example the Gerischer element, which in DRT is hard to resolve, but is usually well treated by dedicated impedance software. Use of the well-developed impedance fitting tools seems more convenient and much more established at this stage in the authors' opinion. For additional analysis, the spectrum from Fig. 3A was also fitted with three R-CPE elements, as presented in Fig. 3E. The obtained fit is also very good in the Nyquist plot, but the back-calculated DRT spectra, presented in Fig. 3F, shows a clear deviation from the DRT of the measured spectra. A new contribution with a peak frequency of ~1.5 Hz can be noticed between the low and higher frequency peaks. Thus the DRT can also be used as an important validation tool for the fitting procedure, and can assist in selecting the proper equivalent circuits.

Based on the data presented in Fig. 3, we selected the following parameters for the DRT analysis of all of the spectra: regularisation parameter $\lambda = 1 \times 10^{-3}$, C^4 Matérn discretisation method, and the regularisation derivative: 2nd-order. In our experience, for this set of data, these are the most reproducible and dependable parameters, which can also be confirmed by the equivalent circuit fitting and back-calculation of the DRT, and the similarity of the original and back-calculated DRT results.

Below, we show the spectra and their respective DRT analyses for varying oxygen concentrations (5%, 20%, and 100%) at 700 °C (Fig. 4) and for varying temperatures (800 °C, 700 °C, and 600 °C) measured in 15% O_2 (Fig. 5). The separate peaks, corresponding to the two R-CPE equivalent processes, have been deconvoluted and inserted in the spectra figures.

The oxygen content has a clear influence on the lower frequency contribution. This contribution is clearly visible for 5% O_2, still noticeable for 20% O_2, and seems to disappear in pure O_2. Also, the ohmic resistance and the higher frequency contribution seem to change with oxygen concentration, but to a lesser extent. The DRT analysis of the presented spectra shows good agreement between the measured and fitted spectra. The characteristic (peak) frequencies for the processes are ~120 Hz and ~1 Hz for the higher and lower frequency contributions, respectively.

The exponents for the CPE elements (denoted here as γ-values) were relatively constant for the two contributions. For the higher frequency contribution, which is an apparently depressed semicircle, the γ-value was ~0.70–0.80, whereas, for the lower frequency contribution, the γ-value was between 0.90 and 1.00. As a general comment, we would like to note that the measured polarisation resistance values are quite low, i.e. only ~10 mΩ cm^2 in 100% O_2 at 800 °C (measured resistance of ~50 mΩ cm^2).

The influence of temperature on the impedance spectra is presented in Fig. 5. Strong temperature activation is visible, the resistance of the higher frequency contribution (R_1-CPE1) changes from ~15 mΩ cm^2 at 800 °C to >250 mΩ cm^2 at 600 °C. The lower frequency contribution seems constant, so its relative magnitude vs. R_1-CPE1 changes. At high temperatures, even at a relatively high oxygen concentration of 15%, the resistance of the first and second elements are comparable.

Together with an ohmic resistance (R_s), the proposed equivalent circuit, consisting of two R-CPE sub-circuits connected in series, fit well to all of the measured spectra (see Fig. 3C). The full equivalent circuit of the symmetrical porous electrode cell is thus (according to Boukamp's notation [56]): $R_s(R_1\text{-CPE1})(R_2\text{-CPE2})$. The sum of R_1-CPE1 and R_2-CPE2 corresponds to the R_{pol}. The obtained values of the parameters of each equivalent circuit element were calculated (resistances and capacitances) and analysed individually in details as a function of oxygen concentration (0.3%–100% O_2) and

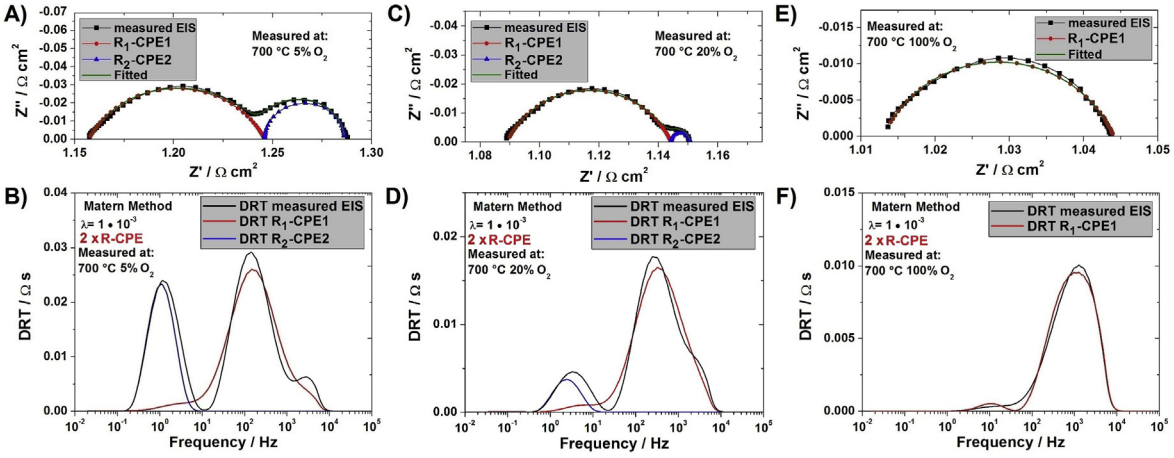

Fig. 4. Impedance spectra measured at 700 °C in different oxygen concentrations and their corresponding DRT plots: A,B) 5% O_2, C,D) 20% O_2, E,F) 100% O_2.

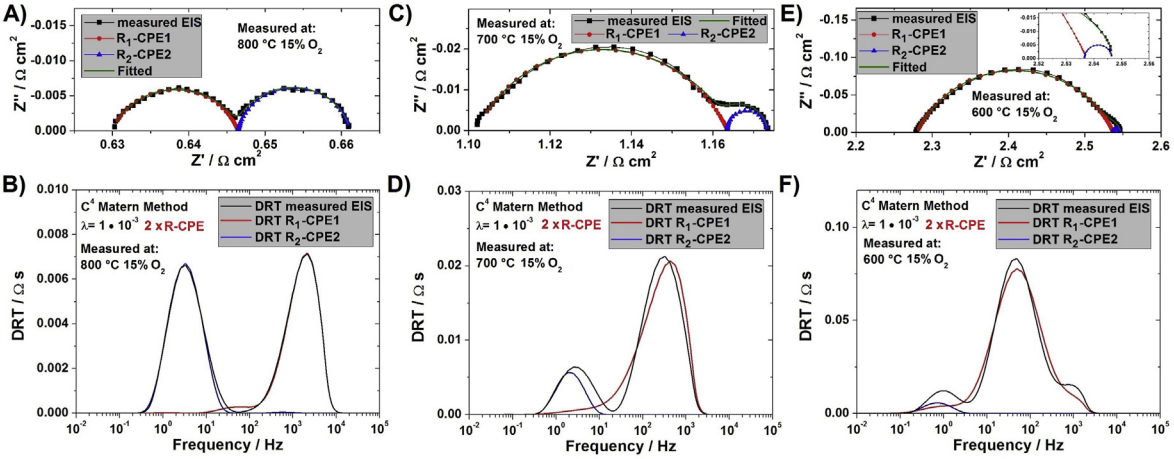

Fig. 5. Impedance spectra measured in 15% O_2 at different temperatures, and their corresponding DRT plots: A,B) 800 °C, C,D) 700 °C, E,F) 600 °C.

temperature (800 °C–500 °C).

3.3. Analysis of ohmic resistance

The ohmic (non-frequency dependent) contribution in the impedance spectra can be the result of several factors. Mainly, it includes the contributions stemming from the electrical conductivity of the thick CGO electrolyte, and of the relatively thin electrodes.

Fig. 6 presents ohmic resistance contribution of the equivalent circuit vs. the oxygen concentration and the temperature. The ohmic resistance changes slightly with the changing oxygen concentration, with a lowering of the resistance at increasing oxygen concentration. This indicates a possible p-type conduction mechanism. The CGO electrolyte, at this pO_2 range, is a pure ionic conductor, so its conductivity can be assumed to be oxygen concentration independent. The electrical conductivity of the STF70 electrode is influenced by the oxygen concentration change, as presented in Fig. 2A. Rothschild et al. showed that the resistivity of STF70 follows the relationship: $R \sim pO_2^{-0.25}$ [42]. Linear fitting of the data shown in Fig. 6 results in slopes in the range −0.03 to −0.05, so much lower than reported for bulk STF70, but it is measured on top of the ceria pellet, which constitutes most of the resistance. Thus the oxygen concentration has a relatively low, but measurable influence on the ohmic resistance of the samples.

The temperature dependence of the conductivity, presented as an Arrhenius plot in Fig. 6B, shows Arrhenius-type temperature-activated behaviour, with activation energy equal to ~0.55 eV. This value is a bit smaller than what was obtained using the van der Pauw method, because the STF70 electrode slightly influences the overall conductivity of the layered structure. This is, however, generally in line with the electrical conductivity activation of ceria-based materials [53,57]. The STF70 has a much lower activation energy and higher conductivity level, and thus the total resistivity is dominated by the CGO.

The ohmic resistance of the CGO at 800 °C, based on the thickness and measured conductivity value (data from Fig. 2A), is ~0.6 Ω cm^2, whereas the ohmic contribution of the STF70 electrodes is only a few mΩ cm^2 at maximum, due to the much higher conductivity and lower thickness. The sum value of ~0.6 Ω cm^2 is very close to the R_s value determined from impedance spectroscopy, which means that no large current constriction/current collection effects take place. The ohmic resistance of the porous electrodes, even in the case of relatively low electric conductivity (assuming a safe, low value of only 10 S cm^{-1} at 800 °C) is very low, below a mΩ cm^2, which represents a negligible value compared to the polarisation resistance, which will dominate the electrode response.

3.4. Analysis of polarisation resistance contributions

Based on the DRT analysis and initial fitting tests, the overall polarisation resistance can be well described by two R-CPE elements for most of oxygen concentrations. For high oxygen content (over 30% O_2), R_2-CPE2 contribution becomes negligible. The relative magnitude of R_1-CPE1 to R_2-CPE2 is very high and fitting by two R-CPE is not possible. In the equivalent circuit used, the higher frequency process, fit to R_1-CPE1, and lower frequency process fit to R_2-CPE2. The determined electrical properties of these elements, determined as a function of oxygen concentration and temperature, are presented in Figs. 7 and 8, respectively.

The higher frequency resistance contribution (R_1) is presented as a function of oxygen concentration in Fig. 7A (see also data in

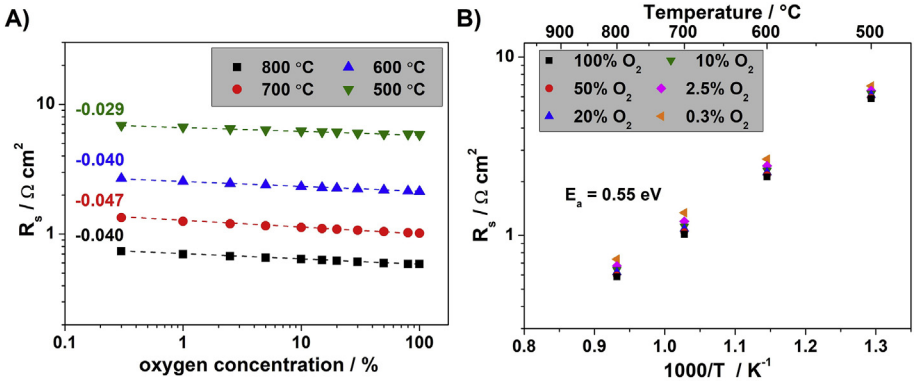

Fig. 6. Ohmic resistance (R_s) of the symmetrical electrodes on CGO as a function of A) oxygen concentration, and B) temperature.

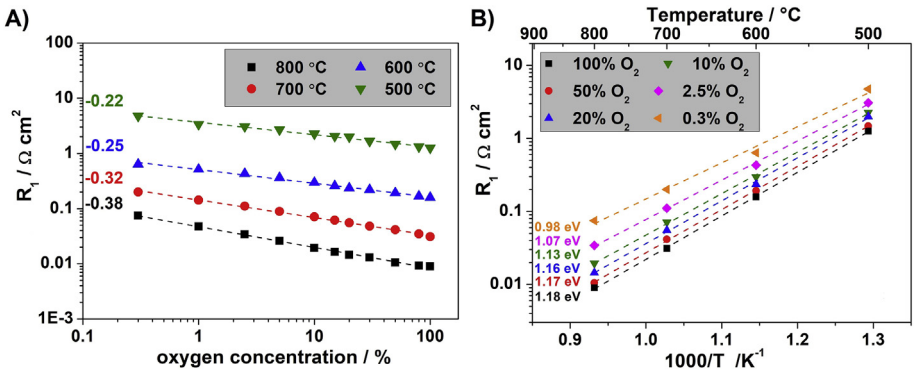

Fig. 7. R_1 resistance values of the symmetrical electrodes on CGO as a function of A) oxygen concentration, and B) temperature.

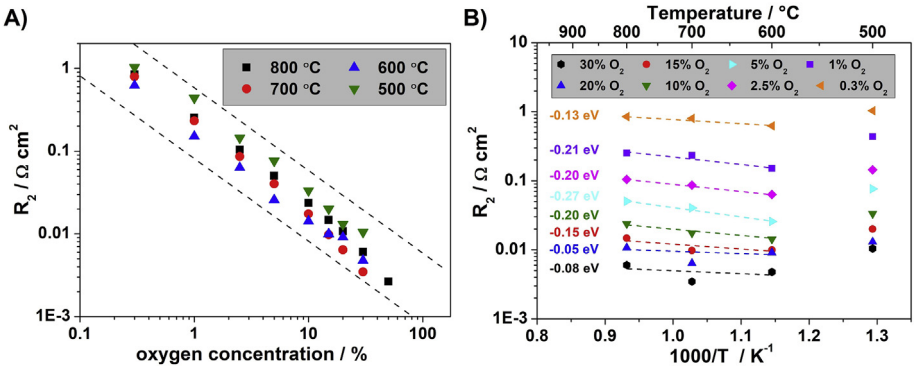

Fig. 8. R_2 resistance values of the symmetrical electrodes on CGO as a function of A) oxygen concentration, and B) temperature.

Table S1). Increasing the oxygen concentration results in decreasing resistance, with the slopes varying in the range $n_{500\ °C} = -0.23$ to $n_{800\ °C} = -0.38$. The dependence on oxygen content can be thus described as moderate. In the lower temperature range (500 °C and 600 °C), the slope values are close to 0.25, which indicates that charge transfer is the rate-determining process (theoretical n = 1/4). For higher temperatures (700 °C and 800 °C), the exponent increases to 0.32–0.38. It is close to a theoretical value of n = 3/8 (0.375) which has been reported to be connected to a reaction controlled by the atomic oxygen diffusion process followed by a charge transfer [58], so a form of intermediate between processes described by n = 1/2 and n = 1/4. The relative change of the limiting processes might be due to different activation energies of the possible contributions (surface diffusion, charge transfer).

Temperature activation of the process described by R_1 is presented in Fig. 7B (see also data in Table S1). The resistance values are dependent on the temperature with an activation energy of ~1.1 eV, slightly dependent on the oxygen concentration. Lowering the oxygen concentration results in lowering the activation energy, from 1.18 eV obtained in 100% O_2 to 0.98 eV in 0.3% O_2.

The obtained data for the R_1 contribution can be compared with our previous results obtained for STF35 [46]. The oxygen dependence slopes were very similar. The resistance magnitude was however higher for the STF35 sample, almost by an order of magnitude. At 800 °C in 20% O_2, the STF35 resistance was ~85 mΩ cm^2, whereas, for the STF70, the resistance was ~14 mΩ cm^2. The lower value of the resistance is due to the faster kinetics of adsorption of oxygen for the iron-richer compound. The temperature effect on the resistance was also stronger for the STF35, for which activation energies ~1.4 eV were reported, considerably higher than the value of 1.1 eV reported here.

The resistance parameters of the second equivalent circuit component, R_2-CPE2, are shown as a function of oxygen concentration in Fig. 8A, and as a function of temperature in Fig. 8B. All results (values of the equivalent circuit parameters) also are collected in Table S1. This is the lowest frequency contribution (characteristic frequency of <5 Hz), clearly noticeable for oxygen concentration < 20%. The strong effect of the oxygen content on the R_2 is visible. The R_2 resistance is directly inversely proportional to the oxygen content. The slope, in the double logarithmic plot, shows inversely proportional behaviour (n = −1). This slope is characteristic for the description of the gas diffusion process in the electrodes. It is thus strongly affected by the oxygen content, but not so much by the temperature, which is evident in Fig. 8B. Due to the relatively low frequency of the process, the fitting at 500 °C can have a relatively large error, thus for the fitting of the activation energy, the three highest temperatures were used. The "activation energy" is negative and has a small magnitude. The values vary between −0.08 and −0.13 eV. If the points at 500 °C were included in the calculation, then the values would be ~0 eV. The low negative temperature effect is also a characteristic feature of the gas diffusion process: in simple theoretical considerations, based on the Nernst equation and gas diffusion laws, Masuda et al. derived a small negative dependence of $T^{-0.5}$ on the gas diffusion overvoltage [59], which is supported experimentally by our results.

To supplement the resistance values, specific pseudo-capacitances and characteristic frequencies of the medium-frequency and low-frequency contributions were calculated, and are presented in Fig. 9A and B, respectively (see also data in Table S2).

For the medium frequency contribution, R_1-CPE1, the specific capacitance (C_1) is in the range 5–144 mF cm^{-2}. Specifically, at

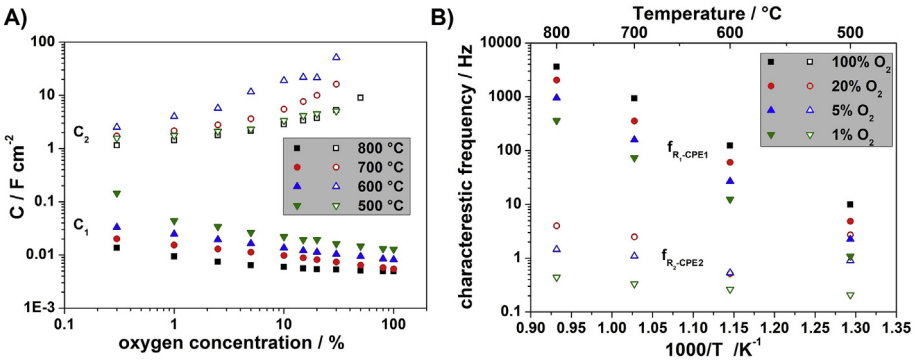

Fig. 9. A) Capacitance, and B) characteristic frequency values calculated from CPE1 and CPE2 contributions.

800 °C, the capacitance varies between 5 and 14 mF cm^{-2} depending on oxygen concentration. The characteristic frequency is strongly affected by the temperature, and also by oxygen concentration. At 800 °C, the characteristic frequency is ~2000 Hz in 20% O_2. Based on the literature, this process can be ascribed to oxygen atom diffusion followed by a charge transfer reaction [58].

For the low-frequency contribution, R_2-CPE2, the specific capacitance shows quite high values. For example, at 500 °C, C_1 varies between ~1.5 F cm^{-2} at 1% O_2, to ~6 F cm^{-2} at 30% O_2. These high capacitance values have a chemical, not electrochemical origin, and are typical for a gas diffusion process. The characteristic frequency of the gas diffusion process is relatively low, ranging from 5 to 0.5 Hz.

Based on the results presented in Figs. 3–9, the values obtained from fitting an equivalent circuit consisting of two R-CPE elements (R_1-CPE1 and R_2-CPE2), corresponding to two possible electrochemical processes, seems valid and well substantiated. The obtained values fit very well with the available literature data reported for mixed ionic electronic conductors.

The porous STF70 electrode shows good electrochemical performance, applicable for practical electrodes for solid oxide cells operating at or above 700 °C, where the polarisation resistance R_{pol} is < 100 mΩ cm^2. This level of polarisation resistance is acceptable for high performance cells, where a polarisation resistance limit of ~150 mΩ cm^2 is often quoted [60]. STF70 is also a Co-free electrode material, which is beneficial from a processing and cost point of view. Also, it has been reported that STF70 has limited Sr surface segregation, so its long-term performance can be favourable [61].

Comparing the obtained results with our previous study of porous STF35 electrodes [46], STF70 shows much higher performance, mostly due to its higher electronic and ionic conductivity, higher surface exchange coefficient (k*) and diffusion coefficient (D*) [36,42]. For STF35, the impedance analysis revealed contributions from the ionic transport in the material (at ~200 Hz) and adsorption (~20 Hz). For STF70, the higher frequency contribution (~2000 Hz at 800 °C) is visible, and the overall polarisation is lower. According to Merkle and Maier, the rate-determining step for Fe-doped $SrTiO_3$ is the dissociation of oxygen, diffusion, and charge transfer, whereas the incorporation into the lattice is a fast process [36]. Clematis et al. analysed the impedance spectra of $Ba_{0.5}Sr_{0.5}Co_{0.8}Fe_{0.2}O_{3-\delta}$ in a 3-electrode setup. The authors describe that at 700 °C, the losses are dominated by ionic conduction and charge transfer at the electrode/electrolyte interface. Oxygen adsorption and bulk diffusion had a minor contribution. The authors did not study the effects of oxygen concentration, but only analysed the polarisation effects. Hjalmarsson and Mogensen analysed symmetrical porous $(La_{0.6}Sr_{0.4})_{0.99}CoO_{3-\delta}$ at different oxygen concentration (2%–100%) [34]. The authors proposed an equivalent circuit consisting of two R-CPE elements in series. The higher frequency contribution (summit frequency of 0.5–5 kHz) showed thermal activation (~1.1 eV), capacitance of ~0.25 mF cm^{-2}, and pO_2 dependence of n = 0.35. The lower frequency contribution was strongly dependent on oxygen concentration and had capacitance values of ~50 mF cm^{-2}, which were ascribed to mass transport limitations (gas diffusion). The origin of a relatively low value of capacitance was unclear. Typically, values of this magnitude are ascribed to molecular adsorption. Wang et al. studied $PrBaCo_2O_{5+x}$ and showed that the major contributions show a charge transfer limitation (n close to 0.25 was obtained) with the characteristic frequency of ~1000 Hz. The polarisation resistance level was quite similar to our work (<125 mΩ cm^2 at 600 °C).

The characteristic frequency value and specific capacitances obtained in this work for the R_1-CPE1 elements differ a bit from the level reported by Escudero et al. [58], but this may be due to much higher performance of the STF70 electrodes, thus shifting the frequency and capacitance values. The activation energy is the same (1.16 eV in the air), and the oxygen concentration dependence is similar.

Our results show that the rate-determining reaction step, at 700 °C and 800 °C is most probably the surface oxygen diffusion process followed by charge transfer. At lower temperatures, i.e. 500 °C and 600 °C, the limiting step is the charge transfer reaction.

4. Conclusions

We studied the electrochemical performance of symmetrical porous $SrTi_{0.30}Fe_{0.70}O_{3-\delta}$ electrodes on a ceria-based electrolyte. Overall, STF70 showed high electrochemical performance (R_{pol} <125 mΩ cm^2 at 600 °C), comparable to state-of-the art materials. We studied a possible electrochemical reaction rate-limiting process by performing impedance measurements as a function of oxygen concentration and temperature. For data analysis, we used the distribution of relaxation times method. The DRT proved to be a useful tool in assisting the selection of a proper equivalent circuit model. Importantly, DRT can also be a very good tool to validate the proposed model by back-calculating the fitted spectra and comparing it with the DRT of the measured one. Based on the analyses, an equivalent circuit composed of two R-CPE elements was selected and fitted to all spectra. The higher frequency process (f_{peak} ~2000 Hz in air at 800 °C), denoted as R_1-CPE1, based on the obtained oxygen concentration dependence of $R \sim pO2^{-0.38}$ was ascribed to originate from surface diffusion of the oxygen species and possible following charge transfer (reduction) reaction. The lower frequency process (R_2-CPE2, f_{peak} ~5 Hz in air at 800 °C) originates from gas diffusion ($R_2 \sim pO_2^{-1}$).

STF70 is a highly performing oxygen electrode material for solid oxide cells, which might find also extensive use in oxygen separation membranes, catalysis, sensors and others. Understanding of the underlying electrochemical processes can lead to further improvement of the material.

This study and the obtained results show that electrochemical impedance spectroscopy, assisted with the distribution of relaxation times data analysis method and extensive temperature and oxygen concentration measurements offer an important insight into the electrochemical processes.

Declaration of competing interest

The authors declare that they have no known competing financial interests or personal relationships that could have appeared to influence the work reported in this paper.

CRediT authorship contribution statement

Aleksander Mroziński: Investigation, Data curation, Visualization, Writing - review & editing. **Sebastian Molin:** Methodology, Writing - original draft, Conceptualization. **Piotr Jasiński:** Resources, Writing - review & editing, Supervision, Funding acquisition, Methodology.

Acknowledgements

This work was partly supported by project funded by National Science Centre Poland based on decision 2017/25/B/ST8/02275. Funding from Statutory Research funds at WETI PG is also acknowledged.

Appendix A. Supplementary data

Supplementary data to this article can be found online at https://doi.org/10.1016/j.electacta.2020.136285.

References

[1] P. Caliandro, A. Nakajo, S. Diethelm, J. Van herle, Model-assisted identification of solid oxide cell elementary processes by electrochemical impedance spectroscopy measurements, J. Power Sources 436 (2019) 226838, https://doi.org/10.1016/j.jpowsour.2019.226838.

[2] A.J. Samson, M. Søgaard, P.V. Hendriksen, Model for solid oxide fuel cell cathodes prepared by infiltration, Electrochim. Acta 229 (2017) 73–95, https://doi.org/10.1016/j.electacta.2017.01.088.

[3] C. Lenser, N.H. Menzler, Impedance characterization of supported oxygen ion conducting electrolytes, Solid State Ionics 334 (2019) 70–81, https://doi.org/10.1016/j.ssi.2019.01.031.

[4] D. Sandil, S. Kumar, K. Arora, S. Srivastava, B.D. Malhotra, S.C. Sharma, N.K. Puri, Biofunctionalized nanostructured tungsten trioxide based sensor for cardiac biomarker detection, Mater. Lett. 186 (2017) 202–205, https://doi.org/10.1016/j.matlet.2016.09.107.

[5] S. Singal, A.K. Srivastava, Rajesh, Electrochemical impedance analysis of biofunctionalized conducting polymer-modified graphene-CNTs nanocomposite for protein detection, Nano-Micro Lett. 9 (2017) 1–9, https://doi.org/10.1007/s40820-016-0108-2.

[6] C. Wei, X. Zou, Q. Liu, S. Li, C. Kang, W. Xiang, A highly sensitive non-enzymatic glucose sensor based on CuS nanosheets modified Cu2O/CuO nanowire arrays, Electrochim. Acta 334 (2020) 135630, https://doi.org/10.1016/j.electacta.2020.135630.

[7] J.L. Song, X. Guo, $SrTi_{0.65}Fe_{0.35}O_3$ nanofibers for oxygen sensing, Solid State Ionics 278 (2015) 26–31, https://doi.org/10.1016/j.ssi.2015.05.009.

[8] L. Folkertsma, L. Gehrenkemper, J. Eijkel, K. Gerritsen, M. Odijk, Reference-electrode free pH sensing using impedance spectroscopy, Proceedings 2 (2018) 742, https://doi.org/10.3390/proceedings2130742.

[9] L. Manjakkal, E. Djurdjic, K. Cvejin, J. Kulawik, K. Zaraska, D. Szwagierczak, Electrochemical impedance spectroscopic analysis of RuO_2 based thick film pH sensors, Electrochim. Acta 168 (2015) 246–255, https://doi.org/10.1016/j.electacta.2015.04.048.

[10] K. Cysewska, L.F. Macía, P. Jasiński, A. Hubin, In-situ odd random phase electrochemical impedance spectroscopy study on the electropolymerization of pyrrole on iron in the presence of sodium salicylate – the influence of the monomer concentration, Electrochim. Acta 290 (2018) 520–532, https://doi.org/10.1016/j.electacta.2018.09.069.

[11] K. Cysewska, M. Gazda, P. Jasiński, Influence of electropolymerization temperature on corrosion, morphological and electrical properties of PPy doped with salicylate on iron, Surf. Coating. Technol. 328 (2017) 248–255, https://doi.org/10.1016/j.surfcoat.2017.08.055.

[12] E. Ivers-Tiffée, A. Weber, Evaluation of electrochemical impedance spectra by the distribution of relaxation times, J. Ceram. Soc. Japan. 125 (2017) 193–201, https://doi.org/10.2109/jcersj2.125.P4-1.

[13] B.A. Boukamp, A. Rolle, Use of a distribution function of relaxation times (DFRT) in impedance analysis of SOFC electrodes, Solid State Ionics 314 (2018) 103–111, https://doi.org/10.1016/j.ssi.2017.11.021.

[14] D. Papurello, D. Menichini, A. Lanzini, Distributed relaxation times technique for the determination of fuel cell losses with an equivalent circuit model to identify physicochemical processes, Electrochim. Acta 258 (2017) 98–109, https://doi.org/10.1016/j.electacta.2017.10.052.

[15] D.A. Osinkin, Complementary effect of ceria on the hydrogen oxidation kinetics on Ni - $Ce_{0.8}Sm_{0.2}O_{2-\delta}$ anode, Electrochim. Acta 330 (2020) 135257, https://doi.org/10.1016/j.electacta.2019.135257.

[16] J. Liu, F. Ciucci, The Gaussian process distribution of relaxation times: a machine learning tool for the analysis and prediction of electrochemical impedance spectroscopy data, Electrochim. Acta 331 (2020) 135316, https://doi.org/10.1016/j.electacta.2019.135316.

[17] X. Li, M. Ahmadi, L. Collins, S.V. Kalinin, Deconvolving distribution of relaxation times, resistances and inductance from electrochemical impedance spectroscopy via statistical model selection: exploiting structural-sparsity regularization and data-driven parameter tuning, Electrochim. Acta 313 (2019) 570–583, https://doi.org/10.1016/j.electacta.2019.05.010.

[18] H. Sumi, H. Shimada, Y. Yamaguchi, T. Yamaguchi, Y. Fujishiro, Degradation evaluation by distribution of relaxation times analysis for microtubular solid oxide fuel cells, Electrochim, Acta 339 (2020) 135913, https://doi.org/10.1016/j.electacta.2020.135913.

[19] F. Ciucci, C. Chen, Analysis of electrochemical impedance spectroscopy data using the distribution of relaxation times: a bayesian and hierarchical bayesian approach, Electrochim. Acta 167 (2015) 439–454, https://doi.org/10.1016/j.electacta.2015.03.123.

[20] M. Saccoccio, T.H. Wan, C. Chen, F. Ciucci, Optimal regularization in distribution of relaxation times applied to electrochemical impedance spectroscopy: ridge and Lasso regression methods - a theoretical and experimental Study, Electrochim. Acta 147 (2014) 470–482, https://doi.org/10.1016/j.electacta.2014.09.058.

[21] T.H. Wan, M. Saccoccio, C. Chen, F. Ciucci, Influence of the discretization methods on the distribution of relaxation times deconvolution: implementing radial basis functions with DRTtools, Electrochim. Acta 184 (2015) 483–499, https://doi.org/10.1016/j.electacta.2015.09.097.

[22] E. Quattrocchi, T.H. Wan, A. Curcio, S. Pepe, M.B. Effat, F. Ciucci, A general model for the impedance of batteries and supercapacitors: the non-linear distribution of diffusion times, Electrochim. Acta 324 (2019) 134853, https://doi.org/10.1016/j.electacta.2019.134853.

[23] F. Ciucci, Modeling electrochemical impedance spectroscopy, Curr. Opin. Electrochem. 13 (2019) 132–139, https://doi.org/10.1016/j.coelec.2018.12.003.

[24] A.P. Tarutin, G.K. Vdovin, D.A. Medvedev, A.A. Yaremchenko, Fluorine-containing oxygen electrodes of the nickelate family for proton-conducting electrochemical cells, Electrochim. Acta 337 (2020) 135808, https://doi.org/10.1016/j.electacta.2020.135808.

[25] S. Wang, H. Jiang, Y. Gu, B. Yin, S. Chen, M. Shen, Y. Zheng, L. Ge, H. Chen, L. Guo, Mo-doped $La_{0.6}Sr_{0.4}Fe_{O3-\delta}$ as an efficient fuel electrode for direct electrolysis of CO_2 in solid oxide electrolysis cells, Electrochim. Acta 337 (2020) 135794, https://doi.org/10.1016/j.electacta.2020.135794.

[26] N. Ortiz-Vitoriano, A. Hauch, I. Ruiz de Larramendi, C. Bernuy-López, R. Knibbe, T. Rojo, Electrochemical characterization of $La_{0.6}Ca_{0.4}Fe_{0.8}Ni_{0.2}O_{3-\delta}$ perovskite cathode for IT-SOFC, J. Power Sources 239 (2013) 196–200, https://doi.org/10.1016/j.jpowsour.2013.03.121.

[27] A. Chrzan, S. Ovtar, P. Jasinski, M. Chen, A. Hauch, High performance $LaNi_{1-x}Co_xO_{3-\delta}$ (x = 0.4 to 0.7) infiltrated oxygen electrodes for reversible solid oxide cells, J. Power Sources 353 (2017) 67–76, https://doi.org/10.1016/j.jpowsour.2017.03.148.

[28] X. Tong, S. Ovtar, K. Brodersen, P.V. Hendriksen, M. Chen, Large-area solid oxide cells with $La_{0.6}Sr_{0.4}CoO_{3-\delta}$ infiltrated oxygen electrodes for electricity generation and hydrogen production, J. Power Sources 451 (2020) 227742, https://doi.org/10.1016/j.jpowsour.2020.227742.

[29] J. Schneider, T. Tichter, P. Khadke, R. Zeis, C. Roth, Deconvolution of electrochemical impedance data for the monitoring of electrode degradation in VRFB, Electrochim. Acta 336 (2019) 135510, https://doi.org/10.1016/j.electacta.2019.135510.

[30] H. Qu, J. Kafle, J. Harris, D. Zheng, J. Koshina, D. Boone, A.M. Drake, C.J. Abegglen, D. Qu, Application of ac impedance as diagnostic tool – low temperature electrolyte for a Li-ion battery, Electrochim. Acta 322 (2019), https://doi.org/10.1016/j.electacta.2019.134755.

[31] S. Sun, Z. Cheng, Electrochemical behaviors for Ag, LSCF and BSCF as oxygen electrodes for proton conducting IT-SOFC, J. Electrochem. Soc. 164 (2017) F3104–F3113, https://doi.org/10.1149/2.0121710jes.

[32] Y. Li, R. Gemmen, X. Liu, Oxygen reduction and transportation mechanisms in solid oxide fuel cell cathodes, J. Power Sources 195 (2010) 3345–3358, https://doi.org/10.1016/j.jpowsour.2009.12.062.

[33] Y. Takeda, Cathodic polarization phenomena of perovskite oxide electrodes with stabilized zirconia, J. Electrochem. Soc. 134 (1987) 2656, https://doi.org/10.1149/1.2100267.

[34] P. Hjalmarsson, M. Søgaard, M. Mogensen, Electrochemical performance and degradation of $(La_{0.6}Sr_{0.4})_{0.99}CoO_{3-\delta}$ as porous SOFC-cathode, Solid State Ionics 179 (2008) 1422–1426, https://doi.org/10.1016/j.ssi.2007.11.010.

[35] L. Navarrete, C. Solís, J.M. Serra, Boosting the oxygen reduction reaction mechanisms in IT-SOFC cathodes by catalytic functionalization, J. Mater. Chem. A. 3 (2015) 16440–16444, https://doi.org/10.1039/c5ta05187h.

[36] R. Merkle, J. Maier, How is oxygen incorporated into oxides? A comprehensive kinetic study of a simple solid-state reaction with SrTiO3 as a model material, Angew. Chem. Int. Ed. 47 (2008) 3874–3894, https://doi.org/10.1002/anie.200700987.

[37] J. Fleig, R. Merkle, J. Maier, The p(O2) dependence of oxygen surface coverage and exchange current density of mixed conducting oxide electrodes: model considerations, Phys. Chem. Chem. Phys. 9 (2007) 2713–2723, https://doi.org/10.1039/b618765j.

[38] W. Jung, H.L. Tuller, Investigation of cathode behavior of model thin-film $SrTi_{1-x}Fe_xO_{3-\delta}$ (x = 0.35 and 0.5) mixed ionic-electronic conducting electrodes, J. Electrochem. Soc. 155 (2008) B1194–B1201, https://doi.org/10.1149/1.2976212.

[39] N.H. Perry, G.F. Harrington, H.L. Tuller, Electrochemical Ionic Interfaces, Elsevier Inc., 2018, pp. 79–106, https://doi.org/10.1016/B978-0-12-811166-6.00004-2.

[40] T. Miruszewski, K. Dzierzgowski, P. Winiarz, S. Wachowski, A. Mielewczyk-Gryń, M. Gazda, Structural properties and water uptake of $STi_{1-x}Fe_xO_{3-x/2-\delta}$, Materials 13 (2020) 965, https://doi.org/10.3390/ma13040965.

[41] S.J. Litzelman, A. Rothschild, H.L. Tuller, The electrical properties and stability of $SrTi_{0.65}Fe_{0.35}O_{3-\delta}$ thin films for automotive oxygen sensor applications, Sensor. Actuator. B Chem. 108 (2005) 231–237, https://doi.org/10.1016/j.snb.2004.10.040.

[42] A. Rothschild, W. Menesklou, H.L. Tuller, E. Ivers-Tiffée, Electronic structure, defect chemistry, and transport properties of $SrTi_{1-x}Fe_xO_{3-y}$ solid solutions, Chem. Mater. 18 (2006) 3651–3659, https://doi.org/10.1021/cm052803x.

[43] P.J. Gellings, H.J.M. Bouwmeester, Ion and mixed conducting oxides as catalysts, Catal. Today 12 (1992) 1–101, https://doi.org/10.1016/0920-5861(92)80046-P.

[44] P.J. Gellings, H.J.M. Bouwmeester, Solid state aspects of oxidation catalysis, Catal. Today 58 (2000) 1–53, https://doi.org/10.1016/S0920-5861(00)00240-6.

[45] S. Molin, W. Lewandowska-Iwaniak, B. Kusz, M. Gazda, P. Jasinski, Structural

and electrical properties of Sr(Ti, Fe)$O_{3-\delta}$ materials for SOFC cathodes, J. Electroceram. 28 (2012) 80–87, https://doi.org/10.1007/s10832-012-9683-x.
[46] A. Mroziński, S. Molin, J. Karczewski, T. Miruszewski, P. Jasiński, Electrochemical properties of porous $Sr_{0.86}Ti_{0.65}Fe_{0.35}O_3$ oxygen electrodes in solid oxide cells: impedance study of symmetrical electrodes, Int. J. Hydrogen Energy 44 (2019) 1827–1838, https://doi.org/10.1016/j.ijhydene.2018.11.203.
[47] R. Moos, W. Menesklou, H.J. Schreiner, K.H. Härdtl, Materials for temperature independent resistive oxygen sensors for combustion exhaust gas control, Sensor. Actuator. B Chem. 67 (2000) 178–183, https://doi.org/10.1016/S0925-4005(00)00421-4.
[48] H.Y. Li, H. Yang, X. Guo, Oxygen sensors based on $SrTi_{0.65}Fe_{0.35}O_{3-\delta}$ thick film with MgO diffusion barrier for automotive emission control, Sensor. Actuator. B Chem. 213 (2015) 102–110, https://doi.org/10.1016/j.snb.2015.02.079.
[49] A. Mroziński, S. Molin, P. Jasiński, Effect of sintering temperature on electrochemical performance of porous $SrTi_{1-x}Fe_xO_{3-\delta}$ (x= 0.35, 0.5, 0.7) oxygen electrodes for solid oxide cells, J. Solid State Electrochem. (2020), https://doi.org/10.1007/s10008-020-04534-0.
[50] A. Mroziński, S. Molin, J. Karczewski, B. Kamecki, P. Jasiński, The influence of iron doping on performance of $SrTi_{1-x}Fe_xO_{3-\delta}$ perovskite oxygen electrode for SOFC, ECS Trans 91 (2019) 1299–1307, https://doi.org/10.1149/09101.1299ecst.
[51] F. Tietz, Thermal expansion of SOFC materials, Ionics 5 (1999) 129–139, https://doi.org/10.1007/BF02375916.
[52] A. Løken, S. Ricote, S. Wachowski, Thermal and chemical expansion in proton ceramic electrolytes and compatible electrodes, Crystals 8 (2018) 365, https://doi.org/10.3390/cryst8090365.
[53] M. Mogensen, N.M. Sammes, G.A. Tompsett, Physical, chemical and electrochemical properties of pure and doped ceria, Solid State Ionics 129 (2000) 63–94, https://doi.org/10.1016/S0167-2738(99)00318-5.
[54] W. Jung, H.L. Tuller, Impedance study of $SrTi_{1-x}Fe_xO_{3-\delta}$ (x = 0.05 to 0.80) mixed ionic-electronic conducting model cathode, Solid State Ionics 180 (2009) 843–847, https://doi.org/10.1016/j.ssi.2009.02.008.
[55] M. Heinzmann, A. Weber, E. Ivers-Tiffée, Advanced impedance study of polymer electrolyte membrane single cells by means of distribution of relaxation times, J. Power Sources 402 (2018) 24–33, https://doi.org/10.1016/j.jpowsour.2018.09.004.
[56] B.A. Boukamp, Electrochemical impedance spectroscopy in solid state ionics: recent advances, Solid State Ionics 169 (2004) 65–73, https://doi.org/10.1016/j.ssi.2003.07.002.
[57] C. Chatzichristodoulou, P.T. Blennow, M. Søgaard, P. V Hendriksen, M.B. Mogensen, Ceria and its use in solid oxide cells and oxygen membranes. Catal. By Ceria Relat. Mater., second ed., 2013, pp. 623–782, https://doi.org/10.1142/9781848169647_0012.
[58] M.J. Escudero, A. Aguadero, J.A. Alonso, L. Daza, A kinetic study of oxygen reduction reaction on La_2NiO_4 cathodes by means of impedance spectroscopy, J. Electroanal. Chem. 611 (2007) 107–116, https://doi.org/10.1016/j.jelechem.2007.08.006.
[59] K. Masuda, A. Kaimai, K. Kawamura, Y. Nigara, T. Kawada, J. Mizusaki, H. Yugami, H. Arashi, Electrochemical reaction kinetics of mixed conducting electrodes on CeO_2-based solid electrolytes, in: Proc. Electrochem. Soc., 1997, pp. 473–482.
[60] B.C.H. Steele, Survey of materials selection for ceramic fuel cells, Solid State Ionics 88 (1996) 1223–1234, https://doi.org/10.1016/0167-2738(96)00291-3.
[61] S.L. Zhang, H. Wang, M.Y. Lu, A.P. Zhang, L.V. Mogni, Q. Liu, C.X. Li, C.J. Li, S.A. Barnett, Cobalt-substituted $SrTi_{0.3}Fe_{0.7}O_{3-\delta}$: a stable high-performance oxygen electrode material for intermediate-temperature solid oxide electrochemical cells, Energy Environ. Sci. 11 (2018) 1870–1970, https://doi.org/10.1039/C8EE00449H.